An Adaptive Control Allocator for Autonomous Vehicles with Parameter Uncertainty

Dong-liang Chen[1] and Guo-ping Liu[2]

Abstract

In this paper, an adaptive control allocation scheme for a class of nonlinear vehicles is proposed considering the parameter uncertainty of the effectors. A reference model is integrated in the framework to overcome the negative effects brought by the parameter uncertainty. The optimum of the solution is discussed for a class of objectives. Stability proof is given. Compared to most existing methods, the conditions to guarantee the stability of the system are relaxed, which is addressed in the theoretical analysis and the experiment. At last, digital simulation and experiment based on a spacecraft simulator are implemented. The results of simulation and experiment validate the effectiveness of the proposed adaptive control allocator.

Keywords

Control Allocation, Parameter Uncertainty, Adaptive, Vehicles

INTRODUCTION

The control allocation problem arises out of over-actuated mechanical systems, which are equipped with more actuators than the degree-of-freedom to be controlled. For over-actuated mechanical systems, the virtual control efforts, i.e., forces and moments, are generated by the redundant actuators. How to distribute the virtual control efforts among redundant actuators leads to the control allocation problem. This problem exists in wide range of applications such as aircrafts[1], [2], spacecrafts[3], automotive vehicles[4] and marine crafts[5].

Due to the redundancy of actuators, additional optimization objectives may be achieved by coordinating the actuators. For example, to minimize fuel consumption under the precondition that the actual control efforts tend to the reference control efforts as close as possible. The control allocation problem covers plants with linear effectors and nonlinear effectors. The linear model of effectors can be adopted when the nonlinearity of the effectors can be neglected. A review of the control allocation problem and feasible solutions is given in [6], basic concepts can be found there and references therein. Both open-loop and close-loop performance indexes of the existing control allocators are analyzed and compared in [7], which provides standards to assess the performance of different control allocators.

The control allocation for plants with nonlinear effectors is investigated in [8] [9], which employs a nonlinear programming method developed from sequential quadratic programming method. Optimal control allocation is adopted incorporating load information feedback to reduce structural load for aircrafts in [10] and [11]. Model predictive control is adopted to solve the control allocation problem when the actuator dynamics is considered in [12], but no parameter uncertainty is included in the model. Control allocation with actuator failure is studied in [13][14][15]and [16].

According to surveys, the control allocation for plants with static parameters has been well studied, but relatively fewer applicable results have been achieved for plants with parameter uncertainty. The uncertainty of the parameters may drive the trajectory of the system off the optimum, or lead to static bias even instability of the system. An inner-loop controller can mitigate the negative effects when the virtual control efforts, that is, forces and torques, are measurable. But the measurement of virtual control efforts needs auxiliary sensors and devices, thus increases the complexity and cost of the system. Therefore the virtual control efforts may not be available in control allocator design in practice. As a result, advanced control allocation algorithms are in need to guarantee the stability of the system and improve the control performance.

There are mainly two methods to handle the parameter uncertainty in control allocator design. The first method is robust control theory [17][18][19][20]. But to apply this method, an upper bound on the norm of the uncertainty, which is sometimes hard to estimate in practice, is assumed. The other important method is the adaptive control theory, which is usually based on a parameter estimator[4][8][21]. This method is very popular in the control allocation design. However, to guarantee the convergence of the estimated parameter to the true value of the underlined parameter, some conditions should be satisfied such as the well known "persistently exciting" condition. In practice, these condition

[1]Dong-liang Chen is with Department of Control Science and Engineering, Harbin Institute of Technology, Harbin 150001, China
[2]Guo-ping Liu is with Faculty of Advanced Technology, University of south Wales, CF37 1DL Pontypridd, U.K.

Corresponding author:
Dong-liang Chen is with Department of Control Science and Engineering, Harbin Institute of Technology, Harbin 150001, China.
Email: 13B904014@hit.edu.cn

may not be satisfied. To cope with the constraints of the existing methods, A model reference adaptive control allocation scheme is proposed in this paper.

In this paper, a novel solution for control allocation problem for plants with parameter uncertainty is proposed. A reference model is integrated to guarantee the stability of the system. Moreover the solution converges to the optimal trajectory asymptotically for a particular class of optimization objectives. The control allocator is tested by digital simulation and experiment. The results of the digital simulation and the experiment validate the effectiveness of the control allocator. Experiments are of importance in controller design, they not only highlight the value of the controller in practical application, but also bring the problems of the algorithm to light. Therefore controllers validated by experiments are of high value in application.

The contributions of this paper are as follows. Firstly, a model reference adaptive control allocator is proposed to mitigate the negative impacts brought by parameter uncertainty of the effectors without measurement or observation of the virtual control effort or estimation of the parameters. In comparison to most existing methods, the conditions to guarantee the asymptotic stability is much relaxed. Secondly, it guarantees that the solution asymptotically converges to the optimal trajectory. At last, experiment on a spacecraft simulator are implemented to validate the effectiveness of the control allocator. Meanwhile, the proposed method is compared to existing methods in digital simulation and experiment, which shows the advantages of the method.

PROBLEM FORMULATION

In this paper, a class of nonlinear vehicles of the following form is considered

$$\dot{x} = f(x,t) + G(\theta)u \tag{1}$$

where $x \in R^n$ is the state of the nonlinear plant, $f : R^n \times [0,\infty) \to R^n$ is a Lipschitz nonlinear function, and $f(0,t) = 0$, $G(\theta) \in R^{n\times m}$ is a function of the unknown parameter vector θ of the actuators, $\theta \in \Theta = \{v|v \in R^m\}$ with Θ the set of parameter vectors, $u \in R^m$ is control input of the actuator, the second term in right-hand side of (1) represents the virtual control effort τ, that is,

$$\tau = G(\theta)u \tag{2}$$

. As $m > n$, system (1) is over-actuated according to the definition of over-actuation.

Since $f(x)$ is a general nonlinear function, many vehicles can be expressed in the form of (1), such as spacecrafts, marine crafts, and etc.

In essence, the parameter vector θ is influenced by the properties of the effectors, such as the drift of the electrical characteristics of the driving circuits, the aging of the mechanical components and the external disturbances. Therefore, these factors can be reflected by θ, which has a explicit physical meaning: the force generated in an infinitely small time element Δt. The total force generated over a time interval $[0, t_1]$ can be expressed as $\int_0^{t_1} \theta dt$.

In this paper, the matrix $G(\theta)$ without all-zero rows is considered, which means every state is directly actuated by control inputs. However the control allocator designed is not limited to this class of vehicles. When the matrix $G(\theta)$ includes all-zero rows, by performing state transformation $\xi = Tx$, where T is a transformation matrix, the control effectiveness matrix can be transformed as:

$$G_r(\theta) = \begin{bmatrix} O \\ G_a(\theta) \end{bmatrix} \tag{3}$$

where $G_r(\theta)$ is the resulted control effectiveness matrix after the transformation, G_a is the control effectiveness matrix corresponding to the actuated states, $O = \{o_{ij}|o_{ij} = 0\}$ is an all-zero matrix corresponding to the un-actuated states. In this case, when assumption 3 is satisfied, replacing the matrix $G(\theta)$ with $G_a(\theta)$, the proposed control allocator is still applicable.

Due to the redundancy of the actuators, auxiliary objectives may be achieved by adjusting the control input u, which is often formulated as a optimal control allocation problem.

For plants of the form (1), the problem is to find a solution u such that the objective

$$\min_u J(t,u,s) \tag{4}$$

subject to

$$\begin{cases} \tau_c - G(\theta)u = s \\ u \in U \end{cases}$$

is optimized, where U is the feasible region of the control input, s is a slack variable. Objective (4) is a generalized objective that may includes the tracking precision of the virtual control effort, the control energy and etc. τ_c is the commanded virtual control effort generated by the higher-level controller.

There are fundamental theoretical results on the optimization problem (4) when the parameter vector θ is known (see [7]). But how to achieve the optimum when parameter is uncertain is still a challenging task.

The following assumptions are made for the sake of the theoretical analysis.

Assumption 1. *The parameters of effectors vary "slowly" in contrast with the control action of the adaptive control allocator, that is,* $\dot{\theta} \approx 0$.

Assumption 2. *The optimal solution for (4) exists for effectors with static parameters* θ_d. *The corresponding control effectiveness matrix is* $G(\theta_d)$.

Assumption 2 indicates that for the optimization problem (4) with static parameter vector θ_d, there exists a feasible solution $u \in U$ such that J is minimized.

Assumption 3. *There exists a high-level controller that stabilizes the nonlinear vehicle (1) around the origin* $x = 0$ *when the parameters of the effectors are static and known. The output of the high-level controller is achievable for both the actual allocator and the reference control allocator, that is, there exists* $u \in U$ *such that* $G(\theta)u = \tau_c$ *and* $G(\theta_d)u_d = \tau_c$.

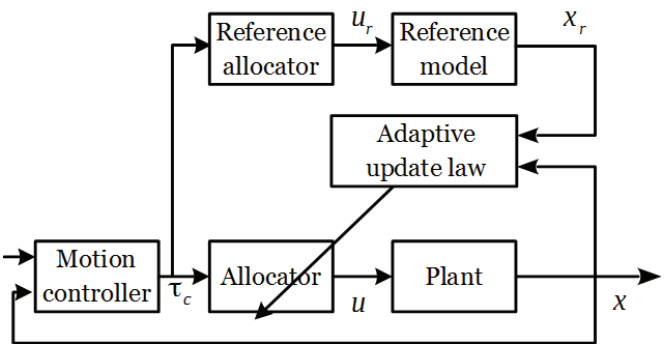

Figure 1. Structure of adaptive control allocation

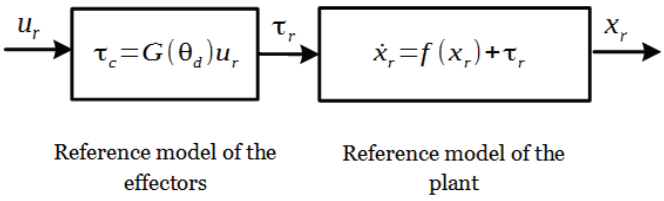

Figure 2. Reference model of the plant

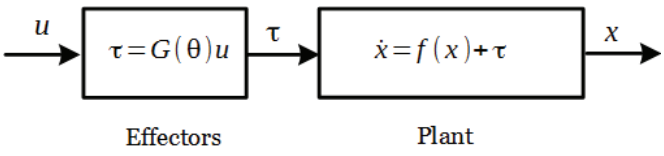

Figure 3. Model of actual plant

An important property of the control effectiveness matrix is to be explored below.

Property 1 The control effectiveness matrix can be decomposed to be $G(\theta) = G_s\Lambda(\theta)$, where $\Lambda(\theta) = diag\,(\theta_1 \quad \theta_2 \quad ... \quad \theta_m)$ is a diagonal matrix. The matrix $G_s = \{g_{ij}|g_{ij} = cos(\phi)\}$ with ϕ the angle between the main axis of the actuator and the corresponding coordinate is a constant matrix determined by the geometrical layout of the actuators.

This property holds if only the actuators of the vehicle are fixed. The example in [22] and the testbed in the experimental section of this paper both satisfy this property. In practice, the actuators are usually installed along the body-fixed axes, in this case, $G_s = \{g_{ij}|g_{ij} = \pm 1\}$.

It can be inferred from property 1 that $\tau = G_s\Lambda(\theta)u = G_s\Lambda(u)\theta$.

Inference 1 The parameter vector in τ is separable, i.e., $\tau = G(\theta)u = H(u)\theta$, where $H(u) \in R^{n\times m}$.

Inference 1 is a straightforward deduction of property 1.

ADAPTIVE CONTROL ALLOCATOR DESIGN

The diagram of adaptive control allocator is illustrated in figure (1).

In figure (1), the motion controller is the aforementioned high-level controller that stabilizes the nonlinear system (1). Its output τ_c is the virtual control effort that is distributed to actuators. When the parameters of effectors are known and time-invariant, the reference virtual control effort τ_c can be achieved instantly and precisely if it is feasible. The nonlinear vehicle (1) is stable accounting for assmption 3. But when the parameters of the effectors drift, the practical control effort τ deviates from the given command τ_c, which will cause bias of x.

The basic idea of our scheme is to design an reference model described by (5) and (6), which gives the reference state vector x_r to measure the bias of the parameters of the effectors,

$$\dot{x_r} = f(x_r) + \tau_c \tag{5}$$

with the reference model of the effector as

$$\tau_c = G(\theta_d)u_r \tag{6}$$

. Based on the information of the bias, the allocator is adjusted by the adaptive update law such that the actual states of the plant converge to the reference states.

The reference allocator aims to solve the following optimization problem:

$$\min_{u_r} J(t, x_r, u_r, s_r) \tag{7}$$

subject to

$$\begin{cases} \tau_c - G(\theta_d)u_r = & s_r \\ u_r \in & U \end{cases}$$

The reference model of the plant is depicted in figure (2). As a comparison,The actual model is depicted in figure (3). It can be seen that the difference between (7) and (4) rely on θ and u. The solution of problem (7) can be achieved utilizing the methods provided by ([6]).

An adaptive update law is designed to regulate the states of the plant x to the reference states x_r. Therefore if the reference system is stabilized by the motion controller, the actual system will also be stabilized.

Writing θ as $\theta = \theta_d + \epsilon$, where $\epsilon \in R^m$ represents the fluctuation of θ. Due to inference 1, the virtual control effort τ can be written as

$$\begin{aligned} \tau = & \quad H(u)\theta \\ = & \quad H(u)(\theta_d + \epsilon) \end{aligned} \tag{8}$$

According to inference 1, the change of control input u can be converted to an equivalent change of θ. So it is reasonable to fix $u = u_r$, meanwhile add a adjustable variable γ to θ, then τ can be rewritten as

$$\tau = H(u_r)(\theta_d + \epsilon + \gamma) \tag{9}$$

Substituting (9) into (1) yields

$$\dot{x} = f(x) + H(u_r)(\theta_d + \epsilon + \gamma) \tag{10}$$

.

In what follows, an adaptive updating law of the adjustable parameter γ is designed such that the trajectory of nonlinear system (10) converges to the trajectory of the reference model (5), i.e., $\lim_{t\to\infty} x(t) = x_r(t)$.

The adaptive updating law of γ is designed as:

$$\begin{cases} H(u_r)\gamma = H(u_r)\delta + f(x_r) - f(x) - K_x\tilde{x} \\ \dot{\delta} = -P^{-1}H^T(u_r)\tilde{x} \end{cases} \tag{11}$$

where K_x, P are positive definite matrices with proper dimensions, $\tilde{x} = x - x_r$ is the state error.

The following theorem guarantees the trajectory of (1) with adaptive control allocator (11) tends to the reference trajectory.

Theorem 1. *The error system $\dot{\tilde{x}} = \dot{x} - \dot{x_r}$ is globally asymptotically stable at the origin with the adaptive control allocator (11) under assumption 1, 2 and inference 1, with K_x and P positive definite matrices, and each entity of K_x is assume to be upper bounded. In addition, the nonlinear system (1) with adaptive control allocator (11) is stable at the origin if assumption 3 holds.*

Remark that the conditions to guarantee the stability of the error system are relaxed compared with the parameter-estimator based algorithms. "Persistently exciting condition" and/or the assumption that the norm of the uncertainty is upper bounded are not necessary to stabilize the overall control system. This is the main feature and advantage of the proposed scheme over most other existing methods.

Proof. Substituting the control allocator (11) into (1) yields the close-loop equation

$$\dot{x} = f(x) + H(u_r)(\theta_d + \epsilon + \delta) + f(x_r) - f(x) - K_x\tilde{x} \tag{12}$$

.

Given the reference model as

$$\begin{aligned} \dot{x_r} = &\quad f(x_r) + G(\theta_d)u_r \\ = &\quad f(x_r) + H(u_r)\theta_d \end{aligned} \tag{13}$$

,

the error system $\dot{\tilde{x}} = \dot{x} - \dot{x}_r$ can be conducted as

$$\begin{cases} \dot{\tilde{x}} = -K_x\tilde{x} + H(u_r)\zeta \\ \dot{\zeta} = -P^{-1}H^T(u_r)\tilde{x} \end{cases} \tag{14}$$

, where $\zeta = \epsilon + \delta$. Due to assumption 1, $\dot{\delta}$ is approximated by $\dot{\delta} = \dot{\zeta}$.

Consider a Lyapunov function $V = \frac{1}{2}\tilde{x}^T\tilde{x} + \frac{1}{2}\zeta^T P\zeta$, whose derivative along the solution of (14) is

$$\begin{aligned} \dot{V} = &\quad \tilde{x}^T(-K_x\tilde{x} + H(u_r)\zeta) + \zeta^T P\dot{\zeta} \\ = &\quad -\tilde{x}^T K_x\tilde{x} + \zeta^T H^T(u_r)\tilde{x} + \zeta^T P\dot{\zeta} \\ = &\quad -\tilde{x}^T K_x\tilde{x} + \zeta^T[H^T(u_r)\tilde{x} + P\dot{\zeta}] \end{aligned} \tag{15}$$

.

For $\dot{\zeta} = \dot{\delta}$ and

$$\dot{\delta} = -P^{-1}H^T(u_r)\tilde{x} \tag{16}$$

, $\dot{V} = -\tilde{x}^T K_x\tilde{x}$ is negative semidefinite, therefore the state vector of (14) is stable, i.e., $\begin{bmatrix} \tilde{x} \\ \zeta \end{bmatrix}$ is bounded.

Differentiating $\dot{V}$ gives

$$\begin{aligned} \ddot{V} = &-(\tilde{x}^T K_x\dot{\tilde{x}} + \dot{\tilde{x}}K_x\tilde{x}) \\ = &\tilde{x}^T(K_xK_x + K_x^TK_x)\tilde{x} - \\ &\tilde{x}^T K_x H(u_r)\zeta - \zeta^T H^T(u_r)K_x\tilde{x} \end{aligned} \tag{17}$$

. Since u_r is bounded, k_{ij} is upper bounded, the boundedness of $\ddot{V}$ can be achieved in conjunction with the stability of $\tilde{x}$ and ζ. According to Barbalat lemma, $\lim_{t\to\infty}\tilde{x} = 0$. The proof is completed.

As there exists a high-level controller that stabilizes the reference nonlinear system (assumption 3), the control allocator (11) stabilizes the reference system x_r. It has been proved previously that the error system $x - x_r$ is stable, thus the control allocator stabilizes the actual system x. This can be achieved by choosing a Lyapunov function as $V_1(x) = V(\tilde{x}) + aV_0(x_r)$, where $V_0 > 0, \dot{V}_0 < 0$ is a Lyapunov function for the close-loop reference system comprised of (5) and a feedback control law $\tau_c = \kappa(x)$, a is a positive number such that the coefficients of $\tilde{x}$ and x_r in $V_1(x)$ are identical. Such feedback control law exists because of assumption 3. It is obvious that the origin of system (1) is stable.

Remark that the stability of the nonlinear system (1) at the origin depends on the stability of the reference nonlinear system (2). For example, if the origin of system (2) is unstable, then the nonlinear system (1) is unstable. However, the nonlinear system (1) is globally stable if only the reference model is locally stable or globally stable. This can be seen from the construction of the Lyapunov function V_1.

Theorem 2. *The control input u given by the control allocator (11) converges to the optimal solution of problem (7) after transients.*

Proof. Theorem 1 guarantees that the actual state x converges to the reference state x_r. Therefore the actual control effort $G(\theta + \gamma)u_r$ converges to $G(\theta_d)u_r$, i.e., $G(\theta + \gamma)u_r \to G(\theta_d)u_r$. Then the slack variable $s \to s_r$. It is a nature conduction that $J(t, x, u, s) \to J(t, x_r, u_r, s_r)$. The proof is completed.

Theorem 1 and 2 guarantee that the control input u converges to the optimal solution of the objective (4) meanwhile stabilizes the nonlinear system (1).

SIMULATION AND EXPERIMENT

In this section, the adaptive control allocator is applied to a planar spacecraft simulator. A path following experiment is designed to test the performance of the adaptive control allocator. The control objective is to drive the spacecraft simulator to a predefined straight line and thereafter moving along the path.

The planar spacecraft simulator is an equipment that is used in ground experiment to simulate the manipulation of spacecrafts operating in outer space. The hardware of the simulator is illustrated in figure (4).

The air-tank is filled with pressured air, which will be provided to the thrusters and the planar air bearings. When the pressured air passes through the planar air bearings, a thin

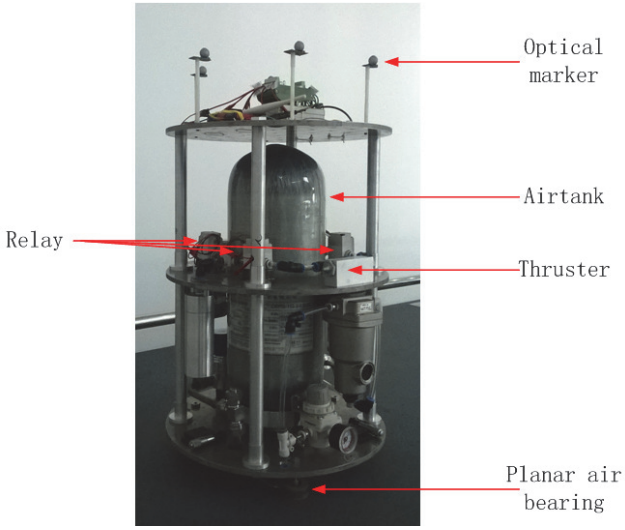

Figure 4. Structure of the spacecraft simulator

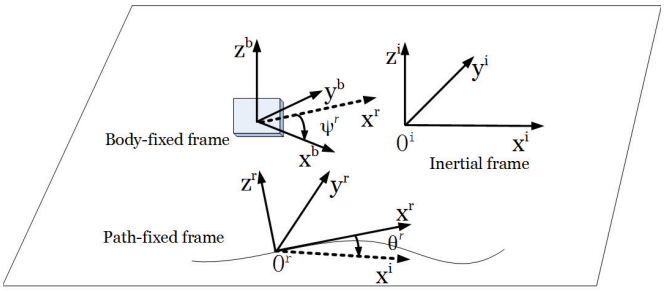

Figure 5. Coordination systems

air film is formed between the air bearings and the marble table such that the motion of the simulator on the table is nearly frictionless. This is the prevailing method to simulate the outer space environment in experiments currently. The simulator is driven by four thrusters. When the pressured air passes through the tiny hole of the thrusters, a opposite action will act on the simulator and then the simulator can move. The relays are used to control the thrusters. The inputs of these relays are PWM signals outputted by the on-board processor. The optical markers are used for the positioning system to locate the simulator.

The coordinate systems used to describe the dynamics of the spacecraft simulator are illustrated in figure (5), i.e., the inertial frame, the path-fixed frame and the body-fixed frame. As the predefined path is a straight line, which is stationary with respect to the inertial frame, the body-fixed frame and the path-fixed frame are sufficient to describe the dynamics of the spacecraft simulator.

Based on rigid body dynamics, the model of spacecraft simulator is derived as follows, detailed derivation can be found in [23].

$$\begin{bmatrix} \nu_x^b \\ \nu_y^b \\ \omega^r \end{bmatrix} = \begin{bmatrix} cos\psi^r & sin\psi^r & 0 \\ -sin\psi^r & cos\psi^r & 0 \\ 0 & 0 & 1 \end{bmatrix} \begin{bmatrix} \dot{x}^r \\ \dot{y}^r \\ \dot{\psi}^r \end{bmatrix} \tag{18}$$

$$\begin{cases} \dot{\nu_x^b} = \dfrac{1}{m}(m\nu_y^b\omega^r + \tau_1) \\ \dot{\nu_y^b} = -\nu_x^b\omega^r \\ \dot{\omega^r} = \dfrac{1}{J}(\tau_2) \end{cases} \tag{19}$$

where (x^r,y^r) are the position of the spacecraft simulator expressed in the path-fixed frame, ψ^r is the orientation of the spacecraft simulator with respect to the path-fixed frame, ν_x^b and ν_y^b are the velocity coordinates of the spacecraft simulator in the body-fixed frame, τ_1, τ_2 are virtual control efforts, i.e., force and torque, respectively, $m = 17.2kg$ and $J = 1.03kg \cdot m^2$ are the mass and the moment of inertia of the spacecraft simulator, respectively.

The model of the effectors is as

$$\begin{bmatrix} \tau_1 \\ \tau_2 \end{bmatrix} = C(\theta)u \tag{20}$$

where $C(\theta) = \begin{bmatrix} \theta_1 & -\theta_2 & \theta_3 & -\theta_4 \\ -R\theta_1 & R\theta_2 & R\theta_3 & -R\theta_4 \end{bmatrix}$ is the control effectiveness matrix, $u \in R^4$ is the control input of actuators, that is, the duty ratio of the driving PWM (Pulse Width Modulation) signal, $u \geq 0$, R is the distance from the point where the thruster acts on the body to the vertical symmetric axis of the spacecraft simulator. The physical meaning of $\theta_i, i = 1, 2, 3, 4$ is the thrust generated by thruster i when the duty ratio of the corresponding pwm signal is $u_i = 1\%$.

The planar spacecraft simulator has 3 variables to control, i.e., (x^r, y^r, ψ^r), while there are four control inputs. Like many practical spacecrafts, the planar spacecraft simulator is a typical over-actuated system.

The model of the simulator (18) and (19) can be expressed in the following compact form:

$$\dot{\chi} = F(\chi) + G_r(\theta)u \tag{21}$$

where $\chi = [x^r \quad y^r \quad \psi^r \quad \nu_y^b \quad \nu_x^b \quad \omega^r]^T$, $G_r(\theta) = \begin{bmatrix} O_{4\times4} \\ G(\theta) \end{bmatrix}$ with $G(\theta) = \begin{bmatrix} 1/m & 0 \\ 0 & 1/J \end{bmatrix} C(\theta)$

For $C(\theta)$ can be decomposed as

$$C(\theta) = \begin{bmatrix} 1 & -1 & 1 & -1 \\ -R & R & R & -R \end{bmatrix} \begin{bmatrix} \theta_1 & 0 & 0 & 0 \\ 0 & \theta_2 & 0 & 0 \\ 0 & 0 & \theta_3 & 0 \\ 0 & 0 & 0 & \theta_4 \end{bmatrix} \tag{22}$$

, property 1 and inference 1 hold true for $G(\theta)$.

The control objective is to manipulate the simulator to a predefined straight line $y^r = 0$ and move along it thereafter at a given velocity v, which can be expressed as:

$$\lim_{t\to\infty} y^r = 0 \tag{23a}$$

$$\lim_{t\to\infty} \dot{x^r} = v \tag{23b}$$

$$\lim_{t\to\infty} \psi^r = 0 \tag{23c}$$

.

To satisfy assumption 3, a high-level motion controller that stabilizes the overall system is designed.

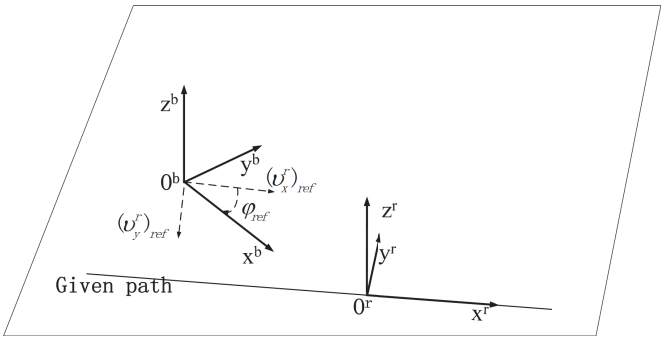

Figure 6. Geometrical illustration of the reference orientation ψ_r

Borrowing the basic idea from [24], the virtual control effort τ_1 is designed as :

$$\tau_1 = -k_1(\nu_x^b - (\nu_x^b)_{ref}) + m(\dot{\nu}_x^b)_{ref} - m\nu_y^b\omega^r \quad (24)$$

, where $k_1 > 0$ is a positive constant, $(\nu_x^b)_{ref}$ is the reference velocity along the x-axis of the body-fixed frame, which is given by (see figure 6 for the geometric explanation)

$$(\nu_x^b)_{ref} = \sqrt{(\nu_x^r)_{ref}^2 + (\nu_y^r)_{ref}^2} \quad (25)$$

being $(\nu_x^r)_{ref} = c$ a predefined constant velocity, and $(\nu_y^r)_{ref}) = -k_4 y^r$ the given velocity along the y-axis of the path-fixed frame.

The other virtual control effort τ_2 is designed as follows to stabilize the orientation loop

$$\tau_2 = -k_2(\omega^r - \omega_{ref}^r) - k_3(\psi^r - \psi_{ref}^r) + J\dot{\omega}_{ref}^r \quad (26)$$

, where the reference orientation ψ_{ref}^r (see figure 6) is given as

$$\psi_{ref}^r = tan^{-1}(\frac{(\nu_y^r)_{ref}}{(\nu_x^r)_{ref}}) = tan^{-1}(\frac{-k_4 y^r}{c}) \quad (27)$$

.

Differentiating ψ_{ref}^r with respect to time in conjunction with equation (18), we get the reference angular velocity ω_{ref}^r

$$\omega_{ref}^r = \frac{-k_4(\nu_y^r)_{ref}^2}{(\nu_x^r)_{ref}^2 + (\nu_y^r)_{ref}^2}(\nu_x^b sin(\psi^r) + \nu_y^b cos(\psi^r)) \quad (28)$$

.

The stability analysis can be accomplished by applying the cascade system theory(see [24]). It is not the emphasis of this paper and therefore not be given here.

The reference control effectiveness matrix is chosen as $G(\theta_d) = \begin{bmatrix} 1.0 & 1.0 & 1.0 & 1.0 \\ 1.0*R & 1.0*R & 1.0*R & 1.0*R \end{bmatrix}$, where $R = 18.5cm$. The performance index of (4) is chosen of the form $J(t,x,u,s) = \sum_{i=1}^{4} u_i$, where s is set to be 0. The linear programming algorithm(see [6] [22] [25]) is adopted to compute the reference control input u_r.

In what follows, digital simulation and experiment are implemented to illustrate the performance of the proposed control allocator. To exhibit the advantages of the proposed method over other methods, two methods are taken as comparison.

Method 1: the linear programming method(see [22] and [25]) is adopted to compute the control input u under nominal value of the parameters, that is, no parameter variation is considered in this case. Therefore $u = u_r$. This method is mainly taken to show the negative effects of the parameter uncertainty on the control performance.

Method 2: the adaptive control allocator based on parameter estimator is designed to handle the parameter uncertainty. The parameter estimator is designed as [26]:

$$\dot{\hat{x}} = f(x,t) + H(u)\hat{\theta} - K_o\tilde{x} \quad (29)$$

$$\dot{\hat{\theta}} = H^T(u)\tilde{x} \quad (30)$$

, with $\hat{x}$ the estimated state, $\hat{\theta}$ the estimated parameter, K_x the gain matrix of the parameter estimator. The gain matrix is designed as $K_o = \begin{bmatrix} 0.9 & 0 \\ 0 & 0.7 \end{bmatrix}$, the initial value of $\hat{\theta}$ is set to be $[0.3 \quad 0.3 \quad 0.3 \quad 0.3]^T$. For the convenience of narration, the method proposed in this paper is denoted as Method 3.

Note that the parameters of the effectors are affected by many factors such as the air flow, the aging of the circuit, and the air pressure variation inside the air tank, thus the uncertainty of the effectors in practice is difficult to model. In digital simulation, a static bias is added to the parameter vector of the effectors as an uncertainty component, while for the experiment the uncertainty is totally unknown. Therefore differences exist between the results of digital simulation and the experiment. Despite of the differences, the simulation and the experiment validate qualitatively the effectiveness of the proposed method.

Simulation

In this section, the adaptive control allocator is implemented and tested in MATLAB/SIMULINK.

The given path is a straight line $y_{ref}^r = 0$, the initial position at time instant $t = 0$ is $\begin{bmatrix} x^r(0) \\ y^r(0) \end{bmatrix} = \begin{bmatrix} 0 \\ -10 \end{bmatrix}$, the commanded velocity along the given path is $0.02m/s$, the given orientation is $\psi^r = 0$. The parameters of the effectors are set as

$$\begin{bmatrix} \theta_1 & \theta_2 & \theta_3 & \theta_4 \end{bmatrix} = \begin{bmatrix} 1.0 & 1.0 & 0.95 & 1.0 \end{bmatrix}$$

, where $\theta_i, i = 1,2,3,4$ is the parameter of thruster i(refer to (20) and its interpretation for the physical meaning). The parameter of θ_3 is set to be smaller than other parameters such that under same driving input signals, thruster 3 generates smaller thrust.

The parameters of the controller and the control allocator are designed as $k_1 = 0.3, k_2 = 0.3, k_3 = 0.1, k_4 = 0.45$ and $K_x = \begin{bmatrix} 1.5 & 0 \\ 0 & 1.5 \end{bmatrix}$, $P^{-1} = \begin{bmatrix} 0.1 & 0 \\ 0 & 0.1 \end{bmatrix}$, respectively.

In figures 7-13, the top subplots show the curves for method 1, the middle subplots show the curves for the control

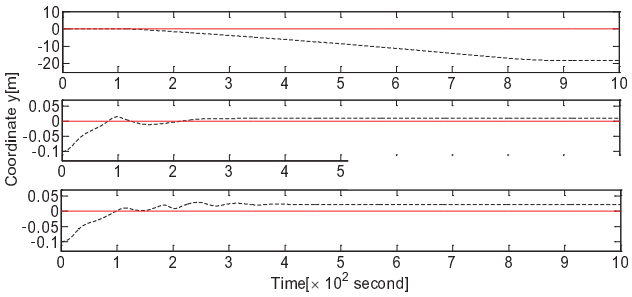

Figure 7. Comparison of coordinate y

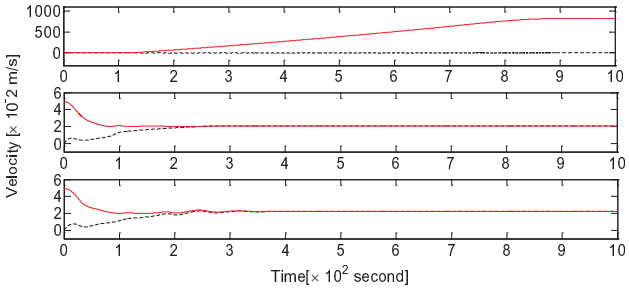

Figure 8. Comparison of forward velocity ν_x^b

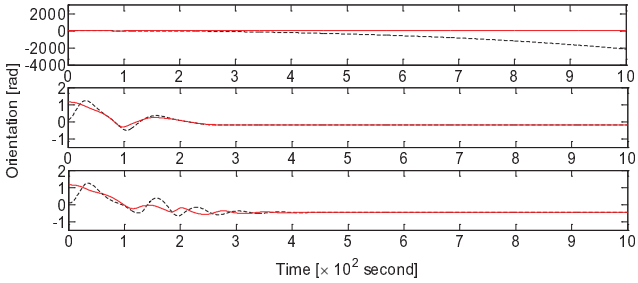

Figure 9. Comparison of angular ψ^r

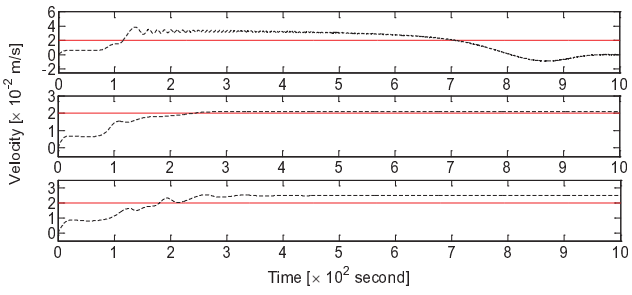

Figure 10. Comparison of velocity along x-direction $\dot{x}^r$

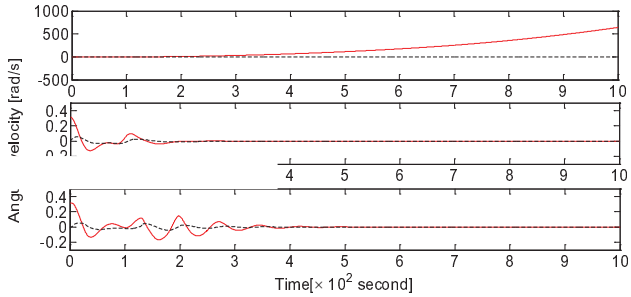

Figure 11. Comparison of the angular velocity ω^r

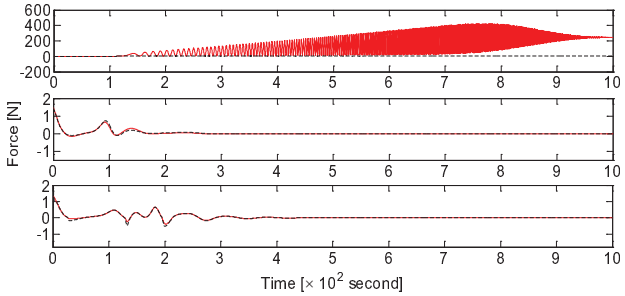

Figure 12. Comparison of control moment τ_1

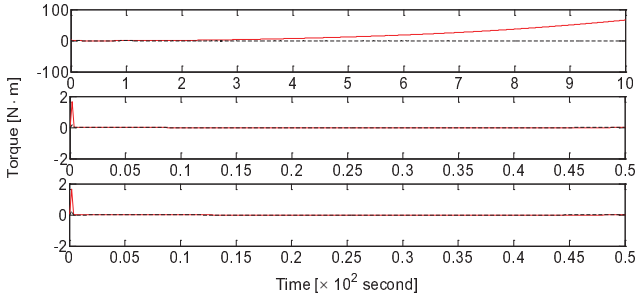

Figure 13. Comparison of control momentτ_2

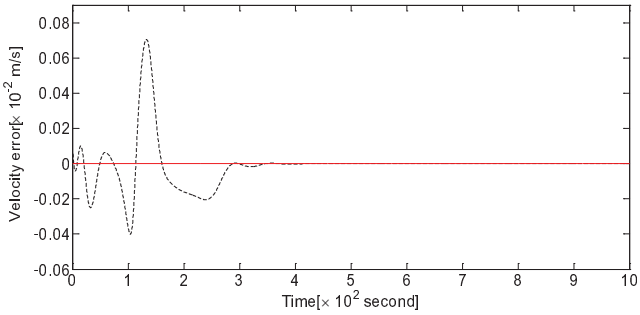

Figure 14. The velocity error $(\nu_x^b)_r - \nu_x^b$ (the dotted line represents the actual trajectory; the valid line represents the reference signal)

allocator proposed in this paper(method 3), while the bottom subplots show the curves for method 2. For all the figures, the valid red lines are the reference signals while the dotted black lines are the actual signals.

Figure 7 shows the trajectory comparison, the static error for non-adaptive control allocator (Method 1) is $-19m$ and $0.025m$ for Method 2, while this error is reduced to $0.01m$ for the proposed adaptive control allocator in this paper(method 3). Other states of the spacecraft simulator,

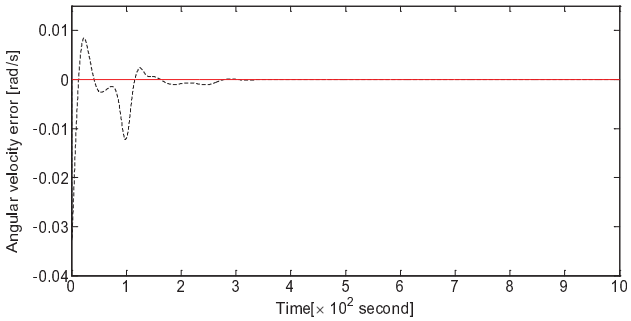

Figure 15. The angular velocity error $\omega_r^r - \omega^r$

e.g., ν_x^b, ψ^r, $\dot{x}^r$, ω_r, are compared in figure 8-11. The responses of these states are important for the overall path-following control performance. In figure 8, it can be seen that ν_x^b converges to the commanded velocity asymptotically for method 2 and method 3, while the static error for method 1 is approximately $8m/s$. In figure 9, a trend that the tracking error keeps increasing can be observed for method 1, which clearly shows that the system is unstable. On the contrary, the tracking error tends to 0 asymptomatically for method 2 and method 3. And it can be seen that the response for method 2 is slower then method 3. From figure 10, one can see that the actual velocity of the simulator oscillates non-periodically around the given velocity at a magnitude of 2 for method 1, while the tracking error decreases to approximately 0.5 for method 2 and this tracking error is further decreased to approximately 0.1 for method 3. The comparison of ω^r is given in figure 11, it is clear that the angular velocity subsystem is unstable without adaptive control allocators. Compared with method 2, the angular response for method 3 is faster. The virtual control effort τ_1, τ_2 are illustrated in figures 12 and 13, respectively. It can be seen from figure 12 that the force vibrates at a high frequency, which indicates much control energy is consumed for method 1. The control energy is smaller for method 3 compared with method 2. Furthermore the actual force tracks the commanded signal accurately and rapidly with the adaptive control allocators while it deviates from the commanded signal without the adaptive control allocators. The improvement brought by the adaptive control allocators is more obvious in figure 13, the actual torque tracks the commanded torque efficiently with the aid of the adaptive control allocators. The state differences between the reference model and the actual model are shown in figure 14 and 15, respectively. It is clear that both $(\nu_x^b)_r - \nu_x^b$ and $\omega_r^r - \omega^r$ converge to origin asymptotically, which verifies the conclusion of theorem 1.

As a conclusion, the simulation results validate that the adaptive control allocators can attenuate the negative effects brought by the parameter uncertainty of effectors significantly. Compared with the adaptive control allocator based on parameter estimators, the control allocator proposed in this paper shows advantages under the experimental setup.

Experiment

In this section, the proposed adaptive allocator is applied to the planar spacecraft simulator(see figure 4).

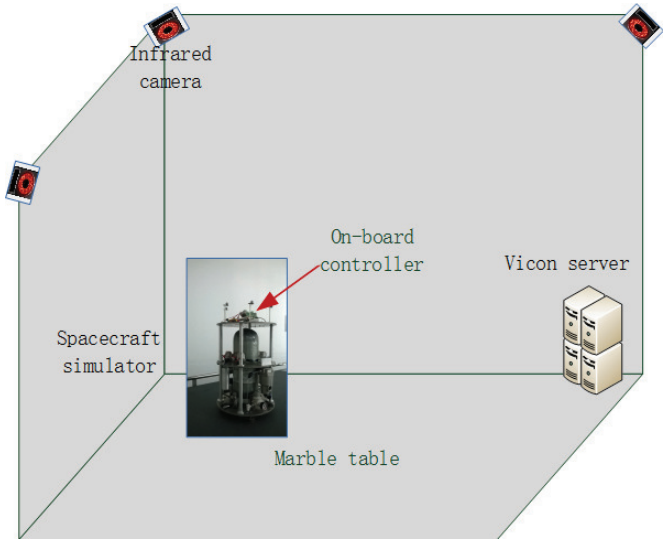

Figure 16. The experimental platform

To implement the proposed control allocator (11), the virtual control effort $H(u_r)\gamma$ in (11) should be distributed to actuators. A transformation algorithm is design to achieve this.

Firstly, γ is expressed as the linear function of θ_d as

$$\gamma = E\theta_d \tag{31}$$

, where E is a diagonal matrix. Since θ_d and γ are known, the matrix E can be computed. Then the left-hand term of (11) can be rewritten as(property 1):

$$H(u_r)\gamma = G(\gamma)u_r \tag{32}$$

.

Substituting 31 to 32, we get

$$\begin{aligned} H(u_r)\gamma &= G(E\theta_d)u_r \\ &= G_s\Lambda(E\theta_d)u_r \\ &= G_s\Lambda(\theta_d)Eu_r \\ &= G(\theta_d)Eu_r \end{aligned} \tag{33}$$

, where property 1 is applied. The new control input Eu_r is added to the control input u_r as the new control input.

The experiment to test the adaptive control allocator is implemented in the laboratory as depicted in figure 16.

The experimental platform comprises three parts. The spacecraft simulator is the controlled plant. Infrared cameras and the vicon server form the positioning system. The on-board processor performs as the controller of the system.

The infrared cameras emit infrared waves, which will be reflected by the optical markers configured on the simulator. Then the reflected waves are captured by the cameras. Based on the information sent from the cameras, the vicon server will compute the coordinates of each optimal marker and send the information to the on-board processor. Utilizing the feedback information sent by vicon server, the on-board processor computes the control input for the actuators, i.e., the relay modules that control the thrusters. A complete motion control system is thus built.

These components are interconnected by the WLAN of the laboratory. The spacecraft simulator operates on a 5m-by-6m polished marble table. A STM32 processor is developed as the on-board controller, its software environment is based on Netconlink, which converts Simulink block diagrams to executable files for STM32. In the software environment, only Simulink block diagrams are needed to implement the control algorithm, which is much easier than C programming. Details of the software environment can be found in [27] and [28].

The given path is $y = 5.2m$, the commanded velocity along the given path is $0.02m/s$, and the commanded orientation is set as $\psi = 0 \quad rad$, i.e., be tangent to the given line. The parameters of the control allocator are given as, $k_1 = 0.3, k_2 = 0.3, k_3 = 0.1, k_4 = 0.45$ and $K_x = \begin{bmatrix} 1.5 & 0 \\ 0 & 1.5 \end{bmatrix}, P^{-1} = \begin{bmatrix} 0.1 & 0 \\ 0 & 0.1 \end{bmatrix}$, respectively.

To simulate the parameter displacement, the actual input for thruster 3 is set to be 75% of the commanded input.

To compare the tracking performances of the three methods quantitatively, three performance indexes are defined.The first performance index is the Absolute Mean Error(AME) $|e_{mean}|$, where e_{mean} is calculated by

$$e_{mean} = \frac{1}{n_2 - n_1} \sum_{k=n_1}^{n_2} (z^s(k) - z_{ref}(k)) \tag{34}$$

. In equation 34, z_s is the steady-state of z, n_1 and n_2 are the starting time and terminal time of the steady-state of z, respectively, z_{ref} is the reference signal. It can be seen from equation 34 that $|e_{mean}|$ represents the tracking precision.

The second performance index is the Absolute Maximal Bias(AMB) $|e_{max}|$, which is defined as:

$$e_{max} = z^s(k_p) - z_{ref} \tag{35}$$

. In equation 35, k_p is the time instant when z reaches its peak after transients. Therefore e_{max} represents the maximal bias of z around the given path.

The third performance index is the Root Mean Square Error(RMSE)[29]

$$e_{rmse} = \sqrt{\frac{1}{n_2 - n_1} \sum_{k=n_1}^{n_2} (z^s(k) - z_{ref}(k))} \tag{36}$$

, which reflects the fluctuation of z around the reference signal z_{ref}.

Figure 17 illustrates the trajectory comparison of the spacecraft simulator.

The three indexes are compared in table 1. The steady-state of the response is defined in this paper as when the curve enters the tube $[5.2 - 0.17, 5.2 + 0.17]$ and stay inside the tube thereafter. It can be seen that the static bias is reduced drastically when the adaptive control allocators(method 2 and method 3) are applied. And compared to method 2, the tracking performance indexes for method 3 except for the RMSE are improved. The fluctuation around the given line for method 2 and method 3 is mainly caused by the fact that ν_y^b in equation (19) is not directly actuated by any control effort. But this phenomenon doesn't exist in the digital simulation, because there is not external disturbances in simulation while the external disturbances are inevitably in practice. The disturbance can cause the simulator deviated from the reference path.

Figure 18 shows the trajectories of the orientation ψ^r. The three indexes are listed in table 2. Except for the index AME, all indexes indicate that a better performance is achieved for method 3 than method 2. In comparison with method 1, method 2 exhibits worse performance, but the mean value of the actual orientation is much closer to the mean value of the reference orientation for method 2 than for method 1.

The velocity ν_x^r, i.e., the velocity along the given line, is illustrated in figure 19. It can be seen from figure 19 that the tracking error is reduced drastically when the adaptive control allocators are applied. The performance index comparison is illustrated in table 3. All performance indexes for method 3 is better than the other two methods. As for the transients, the settling time for method 3 is longer than method 2, but the overshoot is relative smaller than method 2.

In summary, the adaptive control allocator proposed in this paper exhibits competitive control performance according to the digital simulation and experiment over the traditional control allocators. The reason for this advantage is that the conditions to guarantee the stability of this method is relatively relaxed in comparison with the existing methods. Take the parameter-estimator-based allocator as an example, the well-known persistently exciting condition should be satisfied to guarantee the asymptotic stability of the estimator. But this condition is not satisfied as the control inputs of the plants tend to zero after transients (see figure 12 and 13). However this condition is not necessary to guarantee the asymptotic stability for the proposed method here.

CONCLUSION

In this paper, an adaptive control allocator is designed for nonlinear vehicles with parameter uncertainty. Theoretical analysis is given to prove the stability of the overall system with the proposed control allocator. Experiment is implemented to validate the effectiveness of the algorithm.

In future works, the control allocation problem for plants with nonlinear effectors with parameter uncertainty may be considered based on the basic idea of this paper. Furthermore the control allocator developed in this paper may be extended to the case when the dynamics of the actuators is considered. To do this, we need to integrate the underlined dynamics into the reference model.

Acknowledgements

The work is supported by the National Natural Science Foundation of China under Grant 61333003, and by the short-term overseas studying project of Harbin Institute of Technology.

References

[1] David B Doman and Michael W Oppenheimer. Improving control allocation accuracy for nonlinear aircraft dynamics. In *Proceedings of the 2002 Guidance, Navigation and Control Conference*, 2002.

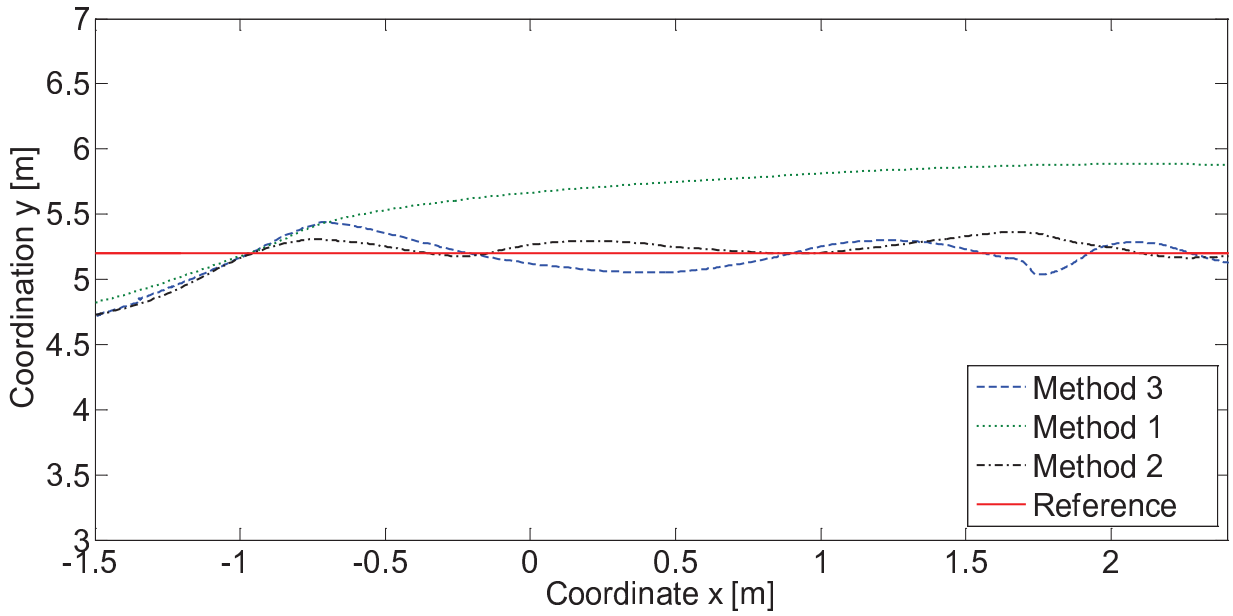

Figure 17. Trajectory comparison with non-adaptive and adaptive control allocator in experiment

Table 1. The trajectory tracking performance comparison

	method 1	method 2	method 3
AME $\lvert e_{mean} \rvert$	0.526	0.046	0.01
AMB $\lvert e_{max} \rvert$	0.685	0.163	0.149
RMSE e_{rmse}	0.557	0.066	0.118

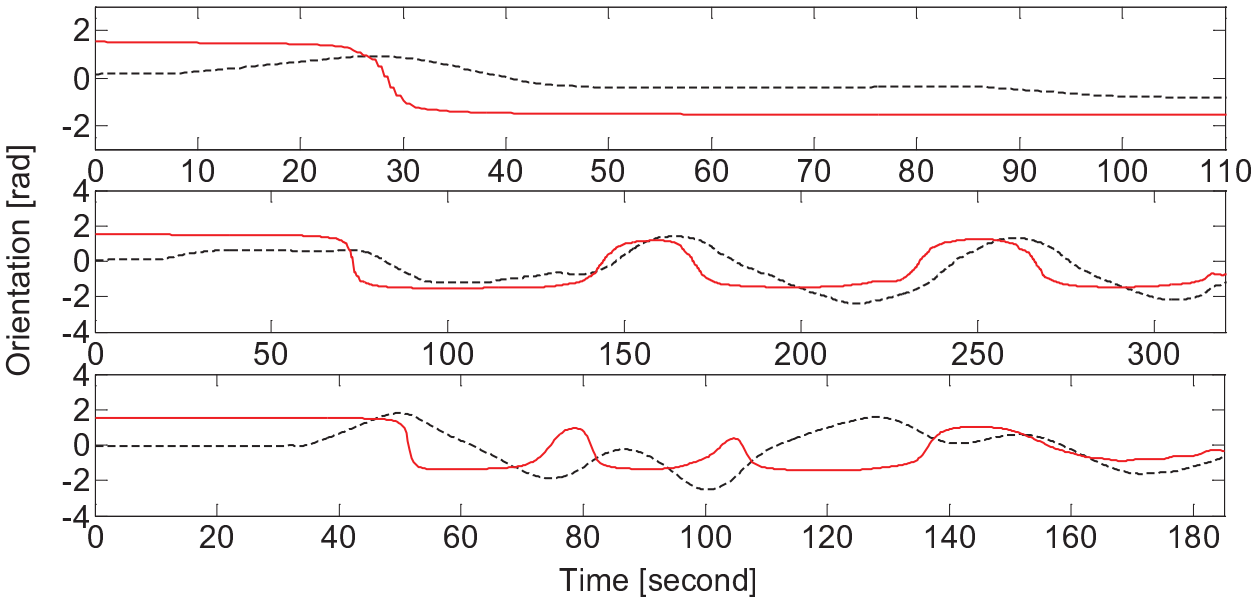

Figure 18. The data history of orientation ψ^r

Table 2. The orientation tracking performance comparison

	method 1	method 2	method 3
AME $\lvert e_{mean} \rvert$	0.6313	0.1337	0.2430
AMB $\lvert e_{max} \rvert$	1.7	3.2	1.7
RMSE e_{rmse}	1.1488	1.4163	1.0107

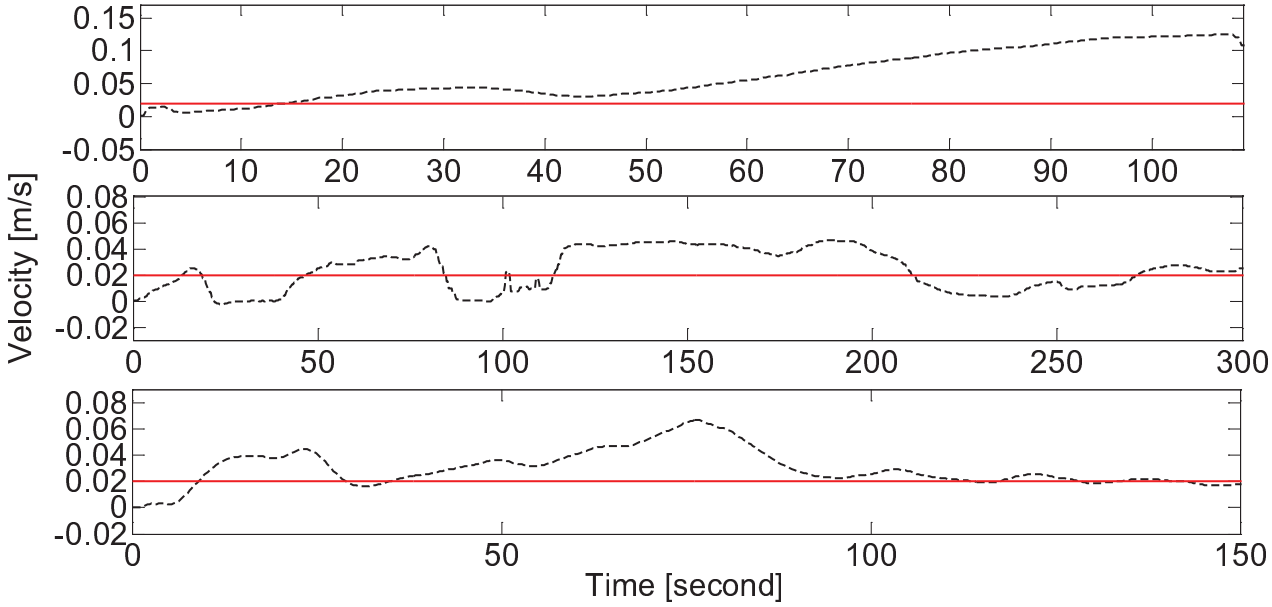

Figure 19. ν_x^r without adaptive control allocator

Table 3. The velocity tracking performance comparison

	method 1	method 2	method 3
AME $\lvert e_{mean} \rvert$	4.1986	0.9599	0.1024
AMB $\lvert e_{max} \rvert$	0.11	0.05	0.025
RMSE e_{rmse}	5.6435	1.6851	1.6047

[2] Yu Luo, Andrea Serrani, Stephen Yurkovich, David B Doman, and Michael W Oppenheimer. Dynamic control allocation with asymptotic tracking of time-varying control input commands. In *American Control Conference, 2005. Proceedings of the 2005*, pages 2098–2103. IEEE, 2005.

[3] David B Doman, Brian J Gamble, and Anhtuan D Ngo. Quantized control allocation of reaction control jets and aerodynamic control surfaces. *Journal of Guidance, Control, and Dynamics*, 32(1):13, 2009.

[4] Johannes Tjonnaas and Tor Arne Johansen. Adaptive optimizing dynamic control allocation algorithm for yaw stabilization of an automotive vehicle using brakes. In *Control and Automation, 2006. MED'06. 14th Mediterranean Conference on*, pages 1–6. IEEE, 2006.

[5] Thor I Fossen and Tor Arne Johansen. A survey of control allocation methods for ships and underwater vehicles. pages 1–6, 2006.

[6] Tor A Johansen and Thor I Fossen. Control allocationła survey. *Automatica*, 49(5):1087–1103, 2013.

[7] Anthony B Page and Marc L Steinberg. A closed-loop comparison of control allocation methods. In *Proc. of AIAA Guidance, Navigation, and Control Conference*, pages 1760–1770, 2000.

[8] Johannes Tjønnås and Tor A Johansen. Adaptive control allocation. *Automatica*, 44(11):2754–2765, 2008.

[9] Thor I Fossen. *Handbook of marine craft hydrodynamics and motion control*. John Wiley & Sons, 2011.

[10] Christopher Miller. Optimal control allocation with load sensor feedback for active load suppression. 2017.

[11] Susan A Frost, Marc Bodson, John J Burken, Christine V Jutte, Brian R Taylor, and Khanh V Trinh. Flight control with optimal control allocation incorporating structural load feedback. *Journal of Aerospace Information Systems*, 2015.

[12] Yu Luo, Andrea Serrani, Stephen Yurkovich, Michael W Oppenheimer, and David B Doman. Model-predictive dynamic control allocation scheme for reentry vehicles. *Journal of Guidance Control and Dynamics*, 30(1):100–113, 2007.

[13] Andrea Cristofaro and Tor Arne Johansen. Fault tolerant control allocation using unknown input observers. *Automatica*, 50(7):1891–1897, 2014.

[14] P Baldi, Mogens Blanke, P Castaldi, N Mimmo, and S Simani. Adaptive ftc based on control allocation and fault accommodation for satellite reaction wheels. In *Control and Fault-Tolerant Systems (SysTol), 2016 3rd Conference on*, pages 672–677. IEEE, 2016.

[15] Mirza Tariq Hamayun, Christopher Edwards, and Halim Alwi. A fault tolerant control allocation scheme with output integral sliding modes. *Automatica*, 49(6):1830–1837, 2013.

[16] Alessandro Casavola and Emanuele Garone. Fault-tolerant adaptive control allocation schemes for

overactuated systems. *International Journal of Robust and Nonlinear Control*, 20(17):1958–1980, 2010.

[17] Qian Wang, Qing Li, Nong Cheng, and Jingyan Song. Robust control allocation method in the presence of control effector failure. In *Information and Automation (ICIA), 2014 IEEE International Conference on*, pages 660–664. IEEE, 2014.

[18] Qinglei Hu, Bo Li, and Aihua Zhang. Robust finite-time control allocation in spacecraft attitude stabilization under actuator misalignment. *Nonlinear Dynamics*, 73(1-2):53–71, 2013.

[19] Aihua Zhang, Qinglei Hu, and Xing Huo. Dynamic control allocation for spacecraft attitude stabilization with actuator uncertainty. *Proceedings of the Institution of Mechanical Engineers, Part G: Journal of Aerospace Engineering*, 228(8):1336–1347, 2014.

[20] Lei Cui and Ying Yang. Disturbance rejection and robust least-squares control allocation in flight control system. *Journal of Guidance, Control and Dynamics*, 34(6):1632–1643, 2011.

[21] Johannes Tjonnas and Tor Arne Johansen. Optimizing adaptive control allocation with actuator dynamics. In *Decision and Control, 2007 46th IEEE Conference on*, pages 3780–3785. IEEE, 2007.

[22] Min Wang and Yongchun Xie. Design of the optimal thruster combinations table for the real time control allocation of spacecraft thrusters. In *Decision and Control, 2009 held jointly with the 2009 28th Chinese Control Conference. CDC/CCC 2009. Proceedings of the 48th IEEE Conference on*, pages 5063–5068. IEEE, 2009.

[23] Vladimir A Chobotov. Spacecraft attitude dynamics and control. *NASA STI/Recon Technical Report A*, 92, 1991.

[24] Signe Moe, Walter Caharija, Kristin Y Pettersen, and Ingrid Schjolberg. Path following of underactuated marine surface vessels in the presence of unknown ocean currents. In *American Control Conference (ACC), 2014*, pages 3856–3861. IEEE, 2014.

[25] Robert J Vanderbei. Linear programming : foundations and extensions. *Journal of the Operational Research Society*, 49(1):93–98, 1998.

[26] Chen Dongliang and Liu Guoping. An adaptive control allocation algorithm for nonlinear vehicles with parameter uncertainty. In *Asia Control Conference*, page accepted. Asian Control Association, 2017.

[27] LIU Guo-Ping, Sun Jian, and ZHAO Yun-Bo. Design, analysis and real-time implementation of networked predictive control systems. *Acta Automatica Sinica*, 39(11):1769–1777, 2013.

[28] Dongliang Chen and Guoping Liu. A real-time networked control framework based on mobile phones. In *Mechatronics and Automation (ICMA), 2015 IEEE International Conference on*, pages 1772–1778. IEEE, 2015.

[29] Hai Peng Ren and Pei Feng Gong. Adaptive control of hydraulic position servo system using output feedback.

Proceedings of the Institution of Mechanical Engineers Part I Journal of Systems & Control Engineering, (3), 2017.

[30] Lawrence R Rabiner, Bernard Gold, and C K Yuen. Theory and application of digital signal processing. *IEEE Transactions on Systems, Man, and Cybernetics*, 8(2):146–146, 1978.